Body-Sound Analysis of a Power-Steering Drive Considering Manufacturing Faults

Christoph Schlensok and Kay Hameyer, *Senior Member, IEEE*

***Abstract*—The acoustic noise and the mechanical behavior of electrical machines gain significance day by day. Applying electrical machines such as induction machines with squirrel-cage rotors (IMs) as power-steering drives in automotive applications requires very strict constraints for the behavior of the motor for both electromagnetic and mechanical means. Therefore, it is of particular interest to analyze the machine's behavior in both means, depending on the technical faults that are caused by manufacturing processes and unavoidable mechanical tolerances. The studied IM is a mass series product and does not allow for expensive manufacturing. Hence, the impact of the technical faults must be estimated and contained. Finite-element models allow for a structured but complex analysis of these tasks.**

***Index Terms*—Body sound, finite-element method (FEM), induction machine, manufacturing faults, power steering, structure dynamics, vibrations.**

I. Introduction

BY APPLYING the finite-element method (FEM), the structure-dynamic behavior of electrical machines has been simulated for several years and is currently the state of the art [1]. The numerical simulation allows for the analysis of both the structure-dynamic and electromagnetic behaviors of the considered machine. With this, the geometry of the machine's structure can be modified, reducing vibrations and hence the radiation of audible noise.

In general, the FEM simulations are performed with "ideal" machines without any defects due to manufacturing tolerances. Here, an induction machine with squirrel-cage rotor (IM) that is applied as a power-steering drive is studied, considering eccentric rotor movement, air enclosures in the rotor bars, balancing kerfs in the rotor teeth, and punching kerfs in the stator teeth. All these defects result from either manufacturing tolerances or the manufacturing process itself. Therefore, consideration of the defects allows for a more detailed analysis of the "real" IM that is employed in its application, i.e., the car. As a reference model, an IM without any of the mentioned defects is computed as well.

The simulation is performed in two steps. In the first step, an electromagnetic model of the IM (one of the five that were listed previously) is applied, followed by the structure-dynamic simulation of a mechanical model of the IM. For the electromagnetic model, the multislice method [2] is applied, allowing for the 2-D simulation of the IM, taking the skewing of the rotor slots into account. This results in a significant speedup of the simulation and provides more exact results than huge and coarse 3-D FEM models by far [3]. Three-dimensional electromagnetic models have been the state of the art up to now.

Manuscript received April 3, 2006; revised September 27, 2006 and December 2, 2006. The review of this paper was coordinated by Dr. B. Fahimi.

The authors are with the Institute of Electrical Machines, RWTH Aachen University, 52056 Aachen, Germany (e-mail: Christoph.Schlensok@iem.rwth-aachen.de).

Digital Object Identifier 10.1109/TVT.2007.896966

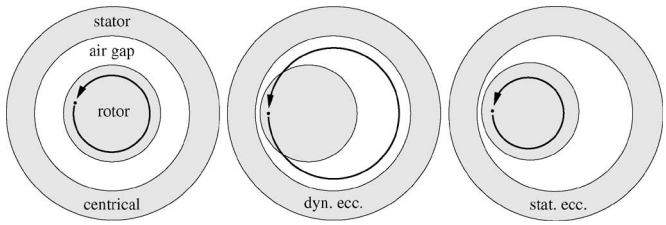

Fig. 1. Types of eccentric rotor movement.

II. Studied Manufacturing Faults

In this paper, four different faults deriving from manufacturing tolerances and processes are studied and compared to an ideal reference model of the IM. The faults are given as follows:

1) eccentric rotor movement;
2) balancing kerfs in the rotor teeth;
3) air enclosures in the rotor bars;
4) punching kerfs in the stator teeth.

The last fault is specific to the studied machine. The other faults are rather common. In fact, any electrical machine is eccentric in some way.

A. Eccentric Rotor Movement

Fig. 1 depicts the three different types of eccentric rotor movement. In general, an electrical machine is designed to be centric, as shown in the leftmost figure. In the case of dynamic eccentricity, the rotor is shifted from the rotational axis and revolves in a whirling motion [4]. The air gap is nonuniform along the circumference. The narrowest air gap revolves with the rotor. If the rotational axis is also shifted from the stator axis, static eccentric rotor movement results. The smallest air gap remains stationary.

B. Balancing Kerfs in Rotor Teeth

Usually, all mechanical parts rotating at higher speeds are balanced to reduce the centrifugal forces. There are several

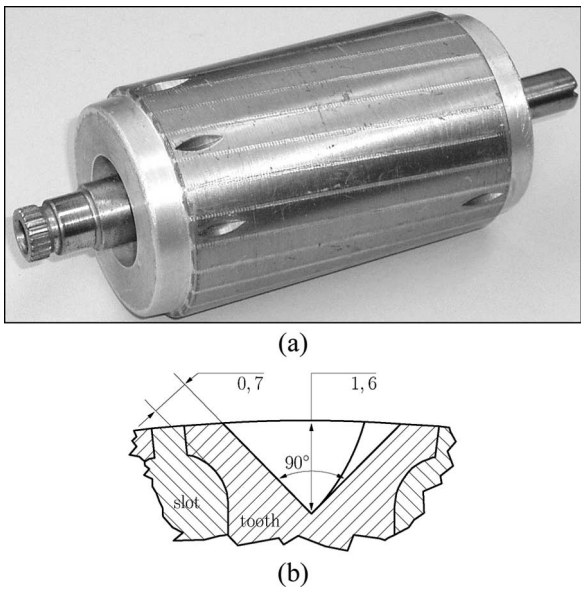

Fig. 2. Balancing kerfs in the rotor teeth. (a) Balancing kerfs in the rotor teeth. (b) Cross section of rotor tooth with balancing kerf.

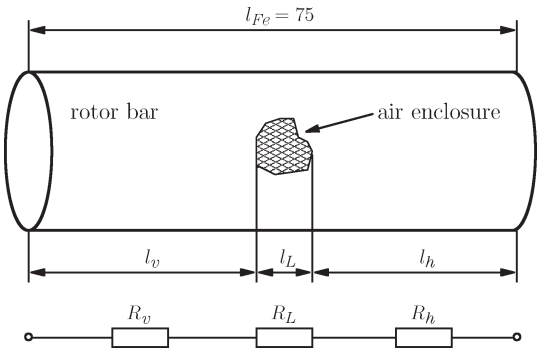

Fig. 3. Air enclosure in the rotor bar.

principles in balancing. Here, the IM is balanced by removing the unbalancing mass from the rotor teeth, as shown in Fig. 2(a). As can be seen, the kerfs only affect about 17% of the axial length of the rotor teeth. However, in this region, they have significant impact to the cross section of the tooth, as depicted in Fig. 2(b).

C. Air Enclosures in Rotor Bars

During the process of die casting, the squirrel cage of the rotor air enclosures are the main occurring fault. The smaller the cross section and the longer the bars get, the higher the risk of air enclosures or even broken rotor bars. The latter one results in nonconducting rotor bars affecting the behavior of the IM significantly. Therefore, there are many studies dealing with the detection of broken bars (Fig. 3) [5].

D. Punching Kerfs in Stator Teeth

This fault, which is special to the studied IM, results from the cheap manufacturing process. Since the air gap between stator and rotor is rather small, the tool for punching the rotor slots

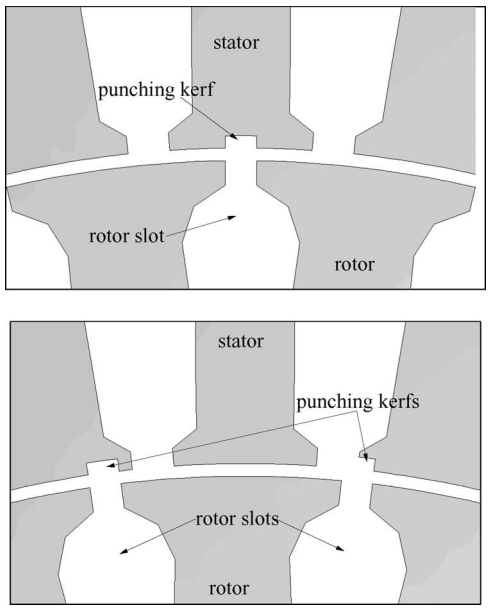

Fig. 4. Punching kerfs in the stator teeth.

reaches into the region of the stator teeth. The studied IM has $N_S = 36$ stator slots and $N_R = 26$ rotor slots. Therefore, the rotor tool cannot be moved to the stator slots, avoiding kerfs in the teeth. As shown in Fig. 4, this results in rectangular kerfs that are distributed asymmetrically along the circumference of the stator lamination.

III. Electromagnetic Simulation

The IM has a three-phase two-layer winding and $2p = 4$ poles. Fig. 5 shows the cross section of the IM. Except for the six mounting kerfs on the outer circumference of the stator, there are no asymmetries. As studies have shown, the impact of the mounting kerfs to the electromagnetic field quantities is negligible. For the electromagnetic model, the region has to be discretized (meshed) continuously. Therefore, the air regions have to be modeled as well. Here, the air gap between stator and rotor ($\delta = 0.3$ mm) and the slot openings are affected. Due to the small air gap and the fact that the electromagnetic energy conversion is performed here, many finite elements have to be arranged in this area. The resulting 2-D model of the IM consists of $N_{\mathrm{el}} = 14\,240$ elements and $N_{\mathrm{node}} = 7194$ nodes.

Since the IM has a squirrel-cage rotor, the rotor-bar currents are unknown. Hence, a transient solver has to be applied for the electromagnetic field problem, taking the rotor movement into consideration [6]–[8]. For the utilization as a power-steering drive, the IM is operated at intermittent duty with long down times. Therefore, the IM requires no explicit cooling and can be operated with high currents and high rotor slip s, respectively. Here, the IM is simulated for operation at a nominal speed of $n = 1200$ r/min, a stator frequency of $f_1 = 48.96$ Hz, and a resulting slip of $s = 18.3\%$.

In the numeric electromagnetic FEM model, speed and currents are switched on at $t = 0$ s. This results in a transient phenomenon of the electromagnetic field values. Exemplarily, the time-dependent behavior of the torque is shown in Fig. 5(b)

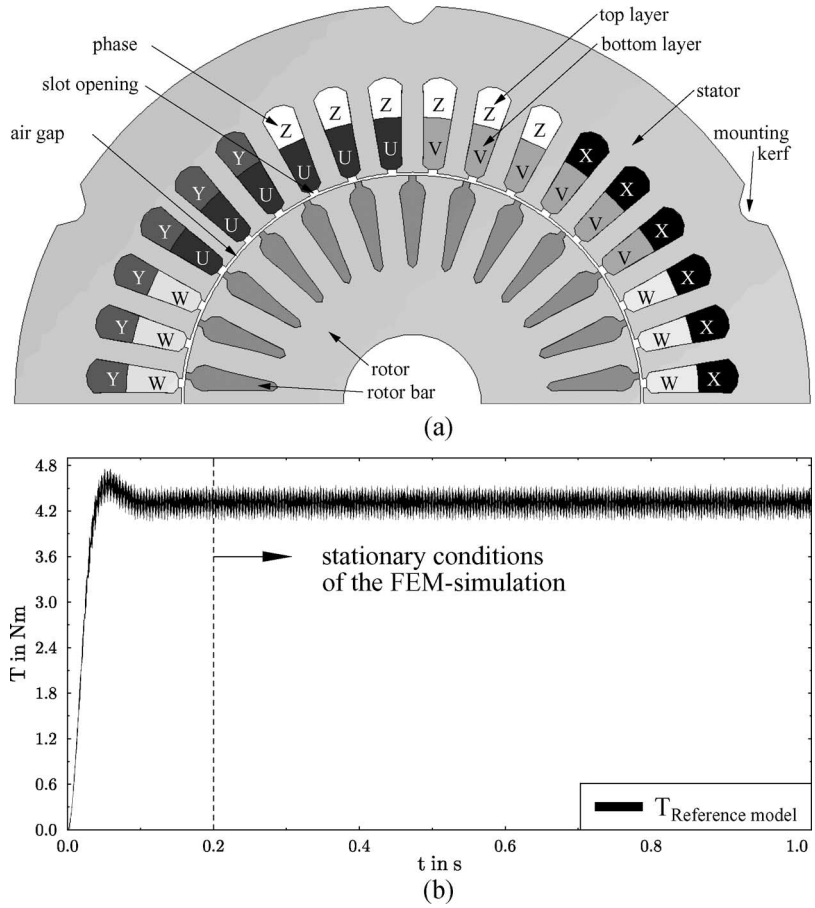

Fig. 5. Cross section of the studied IM. (a) Cross section of the studied IM. (b) Time-dependent torque behavior of the reference model.

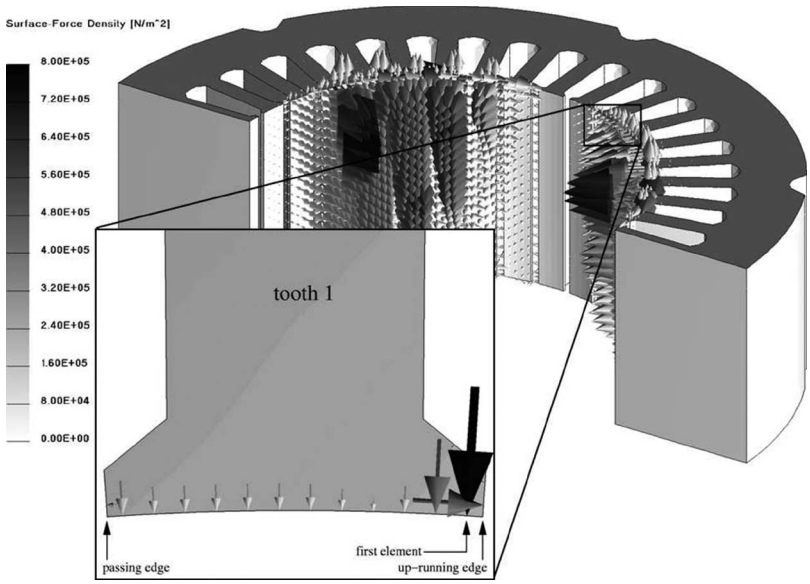

Fig. 6. Surface-force density distribution on the stator of the IM.

for the reference model. After about $T_R = 0.2$ s real time, the transient phenomenon dies out, and stationary conditions are reached. From this point on, the electromagnetic field values can be studied, and secondary values such as torque and forces can be calculated. Here, the net force onto the rotor and the torque are analyzed. For the structure-dynamic analysis of the IM and rotating electrical machines in general, surface-force density σ has to be derived from the flux-density distribution of each transient simulation time step. Therefore, the Maxwell-stress tensor is applied [1].

Fig. 6 depicts the surface-force density on the stator of a 3-D FEM model of the IM and on a single tooth of the 2-D

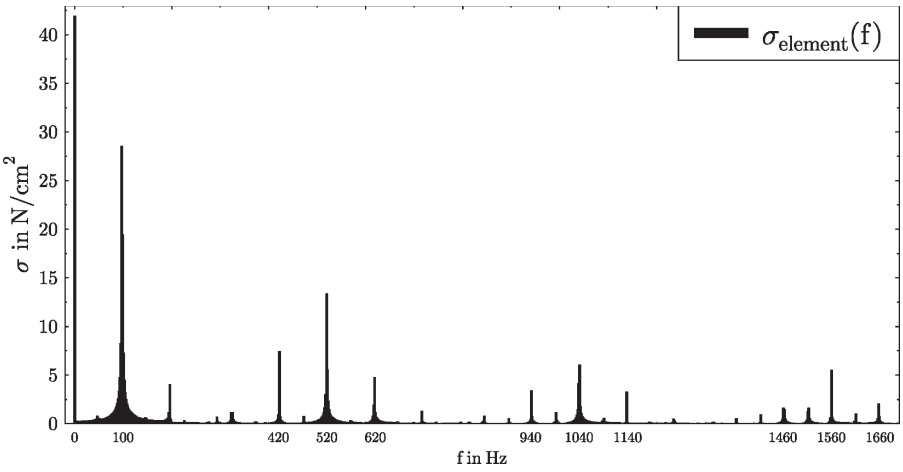

Fig. 7. Spectrum of σ for the reference model.

model. As can be seen, the highest force values are reached at the up-running edge of the teeth. In the case of skewing, the axial force excitation of the stator teeth is also asymmetric. Due to the higher saturation on the upper side of the 3-D stator in the figure, the forces reach higher values as well. The resulting time-dependent surface-force density is transformed to the frequency domain and analyzed. In the following structure-dynamic model, the harmonic forces are used as excitation for the mechanical deformation.

In the following, the net force, torque, and surface-force density of the five models are analyzed. In order to purify the effects of the regarded faults, the skewing of the IM is neglected.

A. Reference Model

The average torque of the IM at the studied point of operation is $\overline{T} = 4.31$ N $\cdot$ m. Slotting and saturation result in oscillating torque contributions. The peak-to-peak value of the torque ripple is $\Delta T = 0.477$ N $\cdot$ m. Skewing, of course, reduces the torque ripple significantly. Due to the even number of rotor slots, the unbalanced magnetic pull on the rotor is zero. Therefore, the net force is $\overline{F} = 0.0$ N as well. For surface-force density σ, the resulting spectrum for a single stator tooth element on the up-running edge is shown in Fig. 7. The occurring harmonics are the double stator frequency

$$2f_1 = 97.92 \text{ Hz} \tag{1}$$

the first, second, and third rotor-slot harmonic

$$i \cdot n = i \cdot 520 \text{ Hz} \qquad \text{for } i = 1, 2, 3 \tag{2}$$

and modulations of the latter one with $2f_1$

$$i \cdot n = i \cdot 520 \pm 2f_1 \text{ Hz} \qquad \text{for } i = 1, 2, 3. \tag{3}$$

B. Eccentric Rotor Movement

In the case of eccentric rotor movement, the maximal manufacturing tolerance for the air gap $v = 0.1$ mm $= 1/3\delta$ is used for the displacement of the rotor. Next to the "pure" eccentric cases, a mixed case (50% dynamic and 50% static eccentricity) is studied. All three models result in nearly the same average torque as that of the reference model. The torque ripple is only affected by the static eccentricity, resulting in $\Delta T = 0.83$ N $\cdot$ m for "pure" static eccentricity and $\Delta T = 0.55$ N $\cdot$ m for the combined model. However, eccentricity results in high unbalanced magnetic pull. Therefore, the average increases drastically. The maximum nearly constant force is reached for the dynamic case: $\overline{F} = 170.2$ N. Static eccentricity results in a pulsating net force ($\overline{F} = 107.4$ N) showing the form of a sinusoidal half-wave. The combined case mixes both behaviors [4], [9]–[11].

For σ, the spectrums differ slightly from the reference model. Some extra frequencies occur. In the case of dynamic eccentricity, this is the order at $n = 20$ Hz (rotor speed). The static eccentricity modulates the existing harmonics with n. Furthermore, in the static case, the stator teeth that are near the location of the smallest air gap are excited more strongly, and on the opposite side of the stator, σ decreases.

C. Balancing Kerfs in Rotor Teeth

The balancing kerfs increase the width of the air gap δ locally, so that the effective air gap for the entire IM is larger than the nominal value. A larger air gap results in lower torque. Thus, the average torque of the IM with balancing kerfs is $\overline{T} = 4.13$ N $\cdot$ m. On the other hand, the machine becomes asymmetric, resulting in higher torque and force oscillation, i.e., $\Delta T = 0.92$ N $\cdot$ m and $\Delta F = 35.2$ N, respectively. The average net force is now $\overline{F} = 22.3$ N. In the neighborhood of the kerfs, σ is affected strongly, as shown in Fig. 8. The edges of the balanced rotor teeth become very small. Therefore, saturation of the iron lamination is reached on both edges. This results in a second up-running edge for the affected teeth, thus increasing the magnitude of the force. Therefore, the rotor-slot harmonics are increased and modulated in the case of balancing kerfs.

D. Air Enclosures in Rotor Bars

In the case of air enclosures in the rotor bars, the variants that are listed in Table I are studied. In all three cases, the

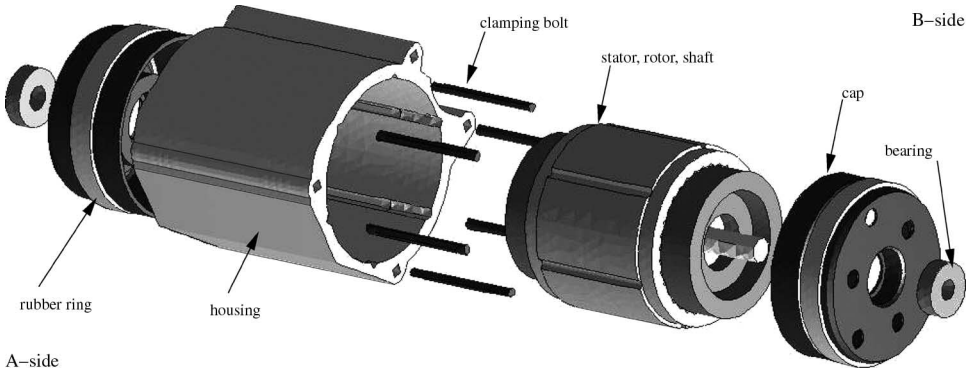

Fig. 8. Doubling effect on σ due to balancing kerfs.

TABLE I
VARIANTS OF THE LOCATION OF THE AIR ENCLOSURES

model	description
1 bar	only one bar is affected
2 next	two neighboring bars are affected
2 opp	two opposite bars are affected

cross section of the air enclosure is varied, taking 10%, 30%, 50%, and 100% of the bars cross section. The last one equals a broken bar.

Only in the case of broken bars is there a significant effect to the IM's average torque. For one broken bar, it decreases to $\overline{T}_{1\,\mathrm{bar}} = 4.17\ \mathrm{N \cdot m}$. Two opposing broken bars reduce the torque to $\overline{T}_{2\,\mathrm{opp}} = 4.12\ \mathrm{N \cdot m}$, while two neighboring broken bars reduce it to $\overline{T}_{2\,\mathrm{next}} = 4.01\ \mathrm{N \cdot m}$. The torque ripple is affected more strongly by the air enclosures. The maximum ripple is now reached for the symmetrical case of two opposing broken bars: $\Delta T_{1\,\mathrm{bar}} = 0.72\ \mathrm{N \cdot m}$ [12]. For the net force, the asymmetric models "1 bar" and "2 next" result in an unbalanced magnetic pull and therefore high average values. The larger the air enclosures, the higher their impact. For broken bars, the maximum is reached: $\overline{F}_{1\,\mathrm{bar}} = 61.9\ \mathrm{N}$ and $\overline{F}_{2\,\mathrm{next}} = 107.3\ \mathrm{N}$.

The surface-force density is not affected in an obvious significant quantity. The deviation of the harmonics is

$$|\sigma_{\mathrm{ref}}(f) - \sigma\ \mathrm{enclosure}(f)| \leq 1.6 \frac{\mathrm{N}}{\mathrm{cm}^2}. \tag{4}$$

E. Punching Kerfs in Stator Teeth

Finally, the impact of the punching kerfs in the stator teeth is studied. Similar to the balancing kerfs, the punching kerfs increase the effective average air gap of the IM. Therefore, the average torque decreases to $\overline{T} = 4.21\ \mathrm{N \cdot m}$. The torque ripple is lifted drastically to $\overline{T} = 1.99\ \mathrm{N \cdot m}$. This is almost 50% of $\overline{T}$. Hence, the performed manufacturing process has a very strong impact here. Due to the symmetry of the punching-kerf distribution, there is no significant effect to the net force.

The deviation of σ depends on the positioning of the kerfs on the regarded stator teeth. If the kerf is positioned at the center, the kerf is rather negligible. However, once the kerfs cut away a piece of the tooth's edge, the magnitudes of the spectrums compared to Fig. 7 increase by about 10% or even more.

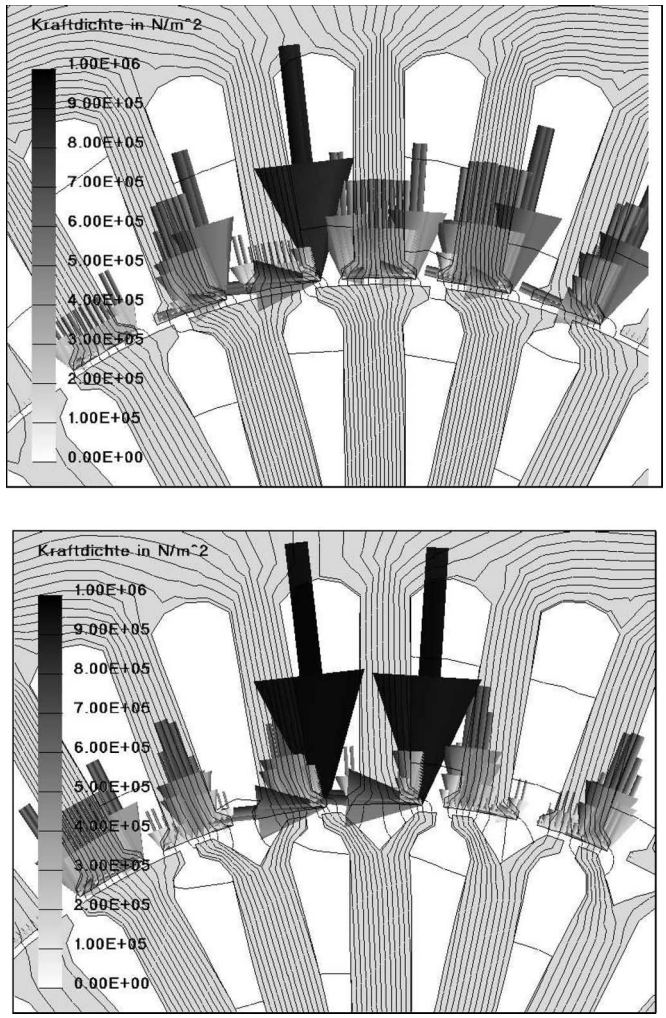

Fig. 9. Mechanical model of the IM.

IV. STRUCTURE-DYNAMIC SIMULATION

In the second step, the mechanical model of the IM simulates the structure dynamically. The mechanical model consists of all mechanical parts of the IM. Fig. 9 shows the rotor and stator with the windings, the housing caps with the bearings, the shaft, and the housing. The stator is fixed to the housing by six pins. The machine is mounted on the front plate of the A side. The B side can oscillate freely, holding the inverter and the control box, which is not modeled here.

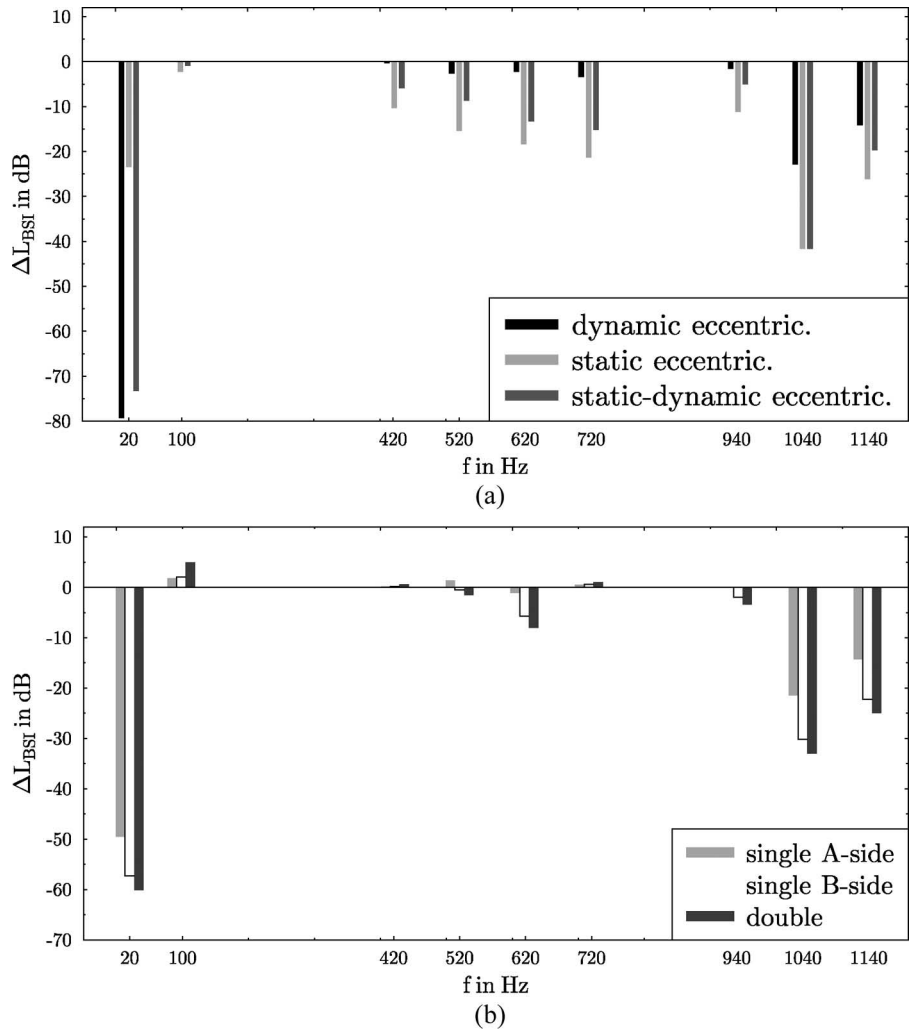

Fig. 10. Deviation of $L_{\mathrm{BSI}}(f)$. (a) Eccentric rotor movement. (b) Balancing kerfs in the rotor teeth.

As our studies have shown, the simulated values of the deformation of the reference model, i.e., the body-sound level, correspond well to measurement results. Unfortunately, the measurement of single separated errors with defined values is very complex and, depending on the error, nearly impossible. In real machines, all errors occur at the same time with different impacts. Stating the error impacts is very difficult. For this, the simulation results of the erroneous models cannot be compared directly to the measurements. Nevertheless, they allow for a detailed analysis of the impact of each of the errors and give hints to optimize the machine's structure-dynamic behavior.

Surface-force density $\sigma(f)$ is transformed from the 2-D electromagnetic model to the 3-D mechanical model. Here, a novel method [3] is applied, accelerating the entire simulation process significantly. $\sigma(f)$ is used as harmonic excitation for the mechanical displacement solver [8]. With the five electromagnetic models from Section III, the mechanical deformation for the frequencies that are detected in Fig. 7 and added by the first stator-slot harmonic at $f = 720$ Hz is computed.

From the deformation, the leveled body-sound index of the housing is analyzed. L_{BSI} is an integral value of the deformation of an entire body, for instance, the housing of the IM. For the nodes of all elements p of the body, the normal component of velocity of deformation $\vec{v}_p$ is summed up. The sum is related to the reference values $S_0 = 1\ \mathrm{m}^2$ and $h_{U_0}^2 = 25 \cdot 10^{-16}\ \mathrm{m}^2/(\mathrm{s}^2)$, and the level is calculated as

$$L_{\mathrm{BSI}}(f) = 10 \log \left(\frac{\sum_{p=1}^{N_{\mathrm{el}}} \int_{S_p} |\vec{v}_p \cdot \vec{n}^p|^2 \, dS}{S_0 \cdot h_{U_0}^2} \right). \qquad (5)$$

$\vec{n}^p$ is the normal vector of element p, f is the frequency, and N_{el} is the number of elements. Therefore, L_{BSI} allows for the evaluation and analysis of a body's entire deformation. For the analysis of the deformation, the results of the $L_{\mathrm{BSI}}(f)$ of the models with manufacturing faults are subtracted from those of the reference model. Hence, negative values represent higher vibrations for the studied model.

A. Eccentric Rotor Movement

In the first step, the eccentric models are studied. As depicted in Fig. 10(a), eccentricity results in higher deformation of the housing for any of the regarded frequencies. In the case of a dynamic portion of eccentricity, the harmonic of the rotor

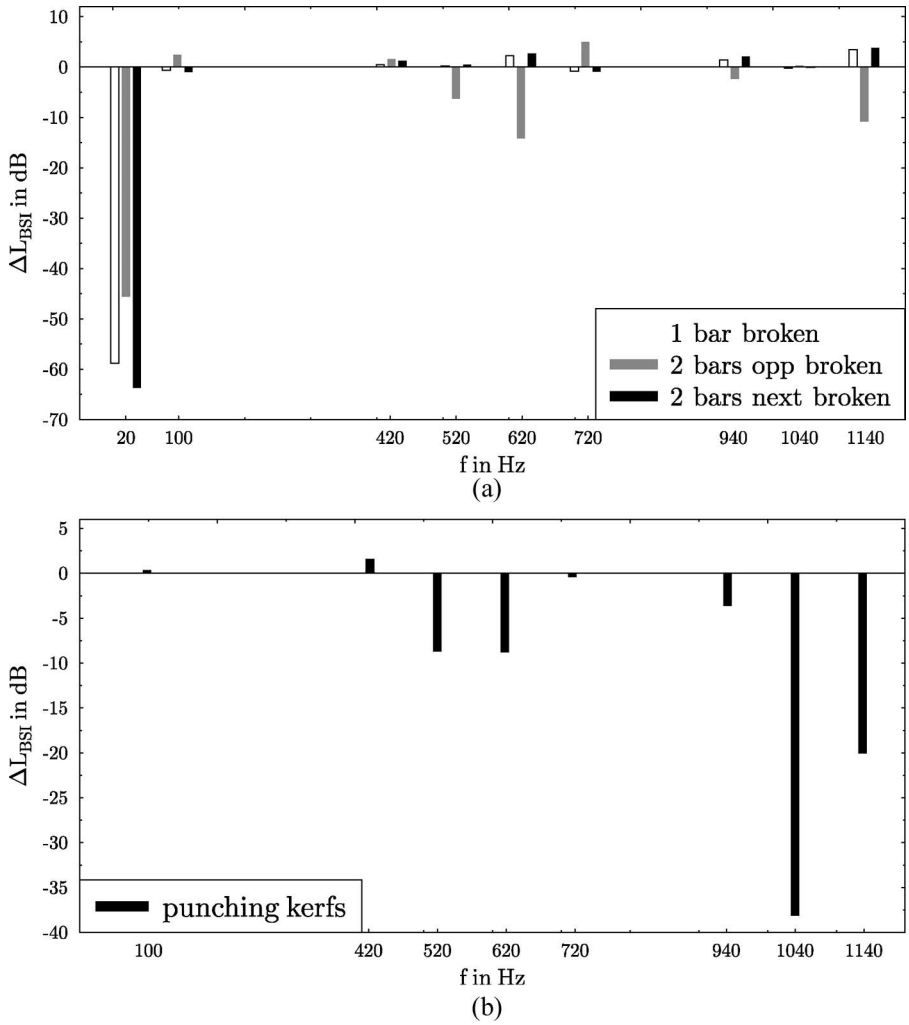

Fig. 11. Deviation of $L_{\mathrm{BSI}}(f)$. (a) Air enclosures in rotor bars. (b) Punching kerfs in the stator teeth.

speed at $f = 20$ Hz is increased up to 80 dB. Nevertheless, the reached level of the body sound is below all of the other harmonics and is therefore neglected.

For all other frequencies, the static eccentricity reaches the highest amplification. For $f = 1040$ Hz, a gain of $\Delta L_{\mathrm{BSI}} = 41.7$ dB is stated. More significant than this is the first stator-slot harmonic at $f = 720$ Hz. Here, the highest overall value of all simulated models is obtained: $L_{\mathrm{BSI}} = 128.0$ dB. This corresponds to measurements and long-term manufacturing experiences: Static eccentricity can cause the highest vibrations due to manufacturing tolerances.

B. Balancing Kerfs in Rotor Teeth

In the case of balancing kerfs in the rotor teeth, the impact is not as significant as that for the eccentric rotor movement [Fig. 10(b)]. Here, the harmonics at rotor speed and the two highest regarded frequencies gain significantly. The maximum amplification is reached at rotor speed for balancing kerfs on both ends of the rotor (marked as "double" in the figure). The gain value is $\Delta L_{\mathrm{BSI}} = 60.2$ dB. Since the resulting absolute level is far below the next higher level of any of the regarded frequencies, the impact is negligible. A higher significance is stated for $f = 1040$ and 1138 Hz. These harmonics lie in the range of frequencies at which the human ear is very sensitive. Both harmonics reach the highest absolute values, except for balancing on the A side (mounted side) of the machine. Therefore, this and the fact of high net force (see Section III) lead to the conclusion, not to balance of the rotor. As measurements on the series IM have shown, the mechanical and acoustic behaviors of the IM have improved significantly, not balancing it.

C. Air Enclosures in Rotor Bars

Air enclosures in rotor bars do not have such a great impact to the mechanical and acoustic noise behaviors of an IM compared to eccentricities or balancing kerfs. For the worst case, i.e., broken bars, the resultant deviation of the body sound is shown in Fig. 11(a). Except for two opposing broken bars, which show some small impact at $f = 520, 618,$ and 1138 Hz, there is no significant excitation of the mechanical structure. As for the two faults that were discussed previously, the huge amplification at rotor speed with up to $\Delta L_{\mathrm{BSI}} = 63.7$ dB results in the smallest absolute level for all of the analyzed harmonics in the spectrum. Therefore, the air enclosures are stated to be less significant for the structure dynamic analysis of induction motors.

TABLE II
SUMMARY OF THE SIMULATION RESULTS

	DE	SE	BK	BBS	BBA	PK
$\overline{T}$			$\downarrow$	$\downarrow$	$\downarrow$	
ΔT		$\uparrow\uparrow$	$\uparrow$	$\uparrow$	$\uparrow$	$\uparrow\uparrow$
$\overline{F}$	$\uparrow\uparrow$	$\uparrow\uparrow$	$\uparrow\uparrow$		$\uparrow\uparrow$	
ΔF	$\uparrow$	$\uparrow\uparrow$	$\uparrow\uparrow$		$\uparrow\uparrow$	
σ						$\uparrow\downarrow$
L_{BSI} general	$\uparrow$	$\uparrow\uparrow$	$\uparrow$	$\uparrow$		$\uparrow$
L_{BSI} at n	$\uparrow\uparrow$		$\uparrow\uparrow$	$\uparrow$	$\uparrow\uparrow$	
$L_{BSI} > 1$ kHz	$\uparrow\uparrow$	$\uparrow\uparrow$	$\uparrow\uparrow$			$\uparrow$

DE: dynamic eccentricity; SE: static eccentricity; BK: balancing kerfs; BBS: broken bars - symmetric; BBA: broken bars - asymmetric; PK: punching kerfs.
$\uparrow,\downarrow$: slight increase, decrease; $\uparrow\uparrow,\downarrow\downarrow$: strong increase, decrease; $\uparrow\downarrow$: depends on frequency.

D. Punching Kerfs in Stator Teeth

Finally, the impact of the punching kerfs in stator teeth is analyzed. Since the punching kerfs are located in the stator teeth, they do not show any impact at rotor speed. Fig. 11(b) shows that the most significant gains can be stated for the second rotor-slot harmonic at $f = 1040$ Hz, with $\Delta L_{\mathrm{BSI}} = 38.1$ dB. The modulated harmonic $f = 1138$ Hz gains $\Delta L_{\mathrm{BSI}} = 20.0$ dB. As mentioned before, this is of particular importance due to the characteristic of the human ear. The absolute levels for both frequencies lie in the same range as those of the models with static eccentricity and balancing kerfs. Therefore, the punching kerfs again (same as for the torque behavior) show a significant impact to the machine's behavior. Nevertheless, due to cost reduction, the series machine is still produced, including punching kerfs.

V. CONCLUSION

In this paper, the body sound of an IM that is applied as a power-steering drive is analyzed, considering manufacturing faults. The impact of eccentric rotor movement, balancing kerfs in the rotor teeth, air enclosures in the rotor bars, and punching kerfs in the stator teeth is studied.

At first, the electromagnetic models are introduced, and the results from numerical FEM simulation are discussed. Torque, net force, and surface-force density show varying impacts, depending on the type of fault that is modeled. Table II summarizes, in qualitative meaning, the results. The average torque $\overline{T}$ is effected by all faults, except for the eccentricities. The torque ripple ΔT is increased by static eccentricity, balancing kerfs, and broken rotor bars. The average net force $\overline{F}$ and the force ripple ΔF rise very strongly for all models, except for the model with two opposing broken rotor bars. In relative quantities, surface-force density σ only shows the impact for punching kerfs and balancing kerfs. In fact, the results of the deformation show that a small deviation of σ might have a great impact.

With the resultant σ as excitation, the deformation of the entire machine structure is simulated, and the level of the body-sound index L_{BSI} is analyzed. For all faults, it can be stated that they have a negative impact to the structure-dynamic behavior of the IM in some way. The strongest impact comes from static eccentricity. Here, the first stator-slot harmonic particularly gains huge quantities. An almost negligible impact is stated for broken rotor bars, resulting in rather small increasing levels.

This paper gives a good overview of four selected faults due to manufacturing tolerances and processes. The results show good accordance to qualitative experienced machine behavior. Measurements of the body-sound level that are performed during series production of the IM reveal the impact of the studied manufacturing effects, for instance, the balancing kerfs. Therefore, it can be stated that the applied method allows for a fast and *a priori* analysis of the regarded manufacturing faults before manufacturing and prototyping. As the case of the balancing kerfs shows (after simulation, the series machine is no longer balanced), the method results in inexpensive and easy solutions for improving machines' acoustics and therefore consumer satisfaction in automotive application.

REFERENCES

[1] I. H. Ramesohl, S. Küppers, W. Hadrys, and G. Henneberger, "Three dimensional calculation of magnetic forces and displacements of a claw-pole generator," *IEEE Trans. Magn.*, vol. 32, no. 3, pp. 1685–1688, May 1996.
[2] J. J. C. Gyselinck, L. Vandevelde, and J. A. A. Melkebeek, "Multi-slice FE modeling of electrical machines with skewed slots—The skew discretization error," *IEEE Trans. Magn.*, vol. 37, no. 5, pp. 3233–3237, Sep. 2001.
[3] C. Schlensok, D. van Riesen, D. Seibert, and K. Hameyer, "Fast structure-dynamic simulation of electrical machines using 2d-3d-coupling," in *Proc. 6th Int. Conf. CEM*, Aachen, Germany, Apr. 2006, p. 34.
[4] A. Tenhunen, T. P. Holopainen, and A. Arkkio, "Effects of saturation on the forces in induction motors with whirling cage rotor," *IEEE Trans. Magn.*, vol. 40, no. 2, pp. 766–769, Mar. 2004.
[5] N. M. Elkasabgy, A. R. Eastham, and G. E. Dawson, "Detection of broken bars in the cage rotor on an induction machine," *IEEE Trans. Ind. Appl.*, vol. 28, no. 1, pp. 165–171, Jan. 1992.
[6] A. Kost, *Numerische Methoden in der Berechnung Elektromagnetischer Felder*. Berlin, Germany: Springer-Verlag, 1994.
[7] O. C. Zienkiewicz and R. L. Taylor, *The Finite Element Method*. London, U.K.: McGraw-Hill Book Company, 1989.
[8] G. Arians, T. Bauer, C. Kaehler, W. Mai, C. Monzel, D. van Riesen, and C. Schlensok, *Innovative Modern Object-Oriented Solving Environment—iMOOSE*, 2006. [Online]. Available: www.imoose.de
[9] A. Tenhunen, "Calculation of eccentricity harmonics of the air-gap flux density in induction machines by impulse method," *IEEE Trans. Magn.*, vol. 41, no. 5, pp. 1904–1907, May 2005.
[10] C. Schlensok and G. Henneberger, "Calculation of force excitations in induction machines with centric and eccentric positioned rotor using 2D Transient FEM," *IEEE Trans. Magn.*, vol. 40, no. 2, pp. 782–785, Mar. 2004.
[11] C. Schlensok, T. Küest, and G. Henneberger, "Comparison of static, dynamic, and static-dynamic eccentricity in induction machines with squirrel-cage rotors using 2D-transient FEM," *COMPEL*, vol. 23, no. 4, pp. 1070–1079, Nov. 2004.
[12] B. Mirafzal and N. A. O. Demerdash, "Diagnosis of eccentricities and bar/end-ring connector breakages in polyphase induction motors through a combination of time-series data mining and time-stepping couples Fe-state-space techniques," *IEEE Trans. Ind. Appl.*, vol. 39, no. 4, pp. 1005–1013, Jul. 2003.

Christoph Schlensok, photograph and biography not available at the time of publication.

Kay Hameyer (M'96–SM'99), photograph and biography not available at the time of publication.